CHEMISTRY OF MATERIALS
Cite This: Chem. Mater. 2019, 31, 9140−9147
Article
pubs.acs.org/cm

Alkyl Phosphonic Acids Deliver $CsPbBr_3$ Nanocrystals with High Photoluminescence Quantum Yield and Truncated Octahedron Shape

Baowei Zhang,[†,‡] Luca Goldoni,[§] Juliette Zito,[†] Zhiya Dang,[†] Guilherme Almeida,[†] Francesco Zaccaria,[†,∥] Jur de Wit,[†,⊥] Ivan Infante,*[,†,∥] Luca De Trizio,*[,†] and Liberato Manna*[,†]

[†]Nanochemistry Department and [§]Analytical Chemistry Lab, Istituto Italiano di Tecnologia, Via Morego 30, 16163 Genova, Italy
[‡]Dipartimento di Chimica e Chimica Industriale, Università degli Studi di Genova, Via Dodecaneso 31, 16146 Genova, Italy
[∥]Department of Theoretical Chemistry, Vrije Universiteit Amsterdam, De Boelelaan 1083, 1081 HV Amsterdam, The Netherlands
[⊥]Utrecht University, Heidelberglaan 8, 3584 CS Utrecht, The Netherlands

Supporting Information

ABSTRACT: We devised a colloidal approach for the synthesis of $CsPbBr_3$ nanocrystals (NCs) in which the only ligands employed are alkyl phosphonic acids. Compared to more traditional syntheses of $CsPbBr_3$ NCs, the present scheme delivers NCs with the following distinctive features: (i) The NCs do not have cubic but truncated octahedron shape enclosed by Pb-terminated facets. This is a consequence of the strong binding affinity of the phosphonate groups toward Pb^{2+} ions. (ii) The NCs have near unity photoluminescence quantum yields (PLQYs), with no need of postsynthesis treatments, indicating that alkyl phosphonic acids are effectively preventing the formation of surface traps. (iii) Unlike NCs coated with alkylammonium or carboxylate ligands, the PLQY of phosphonate coated NCs remains constant upon dilution, suggesting that the ligands are tightly bound to the surface.

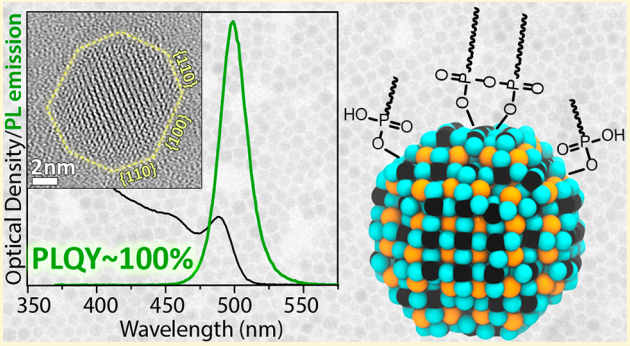

INTRODUCTION

In recent years, lead halide perovskite (LHP) nanocrystals (NCs) have attracted increasing attention due to their excellent optoelectronic properties, which make them particularly interesting for bioimaging,[1] liquid crystal displays,[2] light emitting diodes (LEDs),[3,4] and solar concentrators.[5−7] The initial syntheses of LHP were characterized by the combined use of oleic acid and oleylamine, and the corresponding NCs exhibited poor colloidal stability and limited photoluminescence (PL) quantum yield (QY).[8−11] Such features stem from the presence of labile ligands such as oleylammonium−halide or Cs−oleate species on the surface of LHP NCs.[11−13] These ligands can easily dissolve in neutral solvents because the alkylammonium (oleate) ions can easily lose (gain) a proton in favor of their counterion becoming electrically neutral. To improve the stability of perovskite NCs and to achieve a better surface passivation, different types of ligands have been employed in either postsynthesis ligand exchange procedures (including the use of softer Lewis acids[14] and quaternary ammonium salts[10,15,16]) or directly during the synthesis of perovskite NCs.[17,18] As a notable example, Krieg et al. prepared $CsPbX_3$ NCs with high stability and high PLQY by replacing oleylamine and oleic acid with zwitterionic molecules, which can coordinate to both surface cations and anions and are not subjected to the loss (or gain) of protons.[17] Also, recently Yang et al. demonstrated that sulfonic acids, if employed as the only ligands in the colloidal synthesis of $CsPbBr_3$, lead to stable NCs, which are resistant to both washing procedures with polar solvents and long-term storage under air.[18]

Similarly to sulfonic acids, alkyl phosphonic acids (PAs) should be ideal ligands for the synthesis of LHP NCs, thanks to their strong affinity toward Pb^{2+} ions.[19] Indeed, it has already been observed that the addition of PAs (either as ancillary ligands in the synthesis or during postsynthesis treatments) led to LHP NCs with good PLQY and improved resistance against heating and exposure to air.[14,20−23] Still, a clear understanding of the role of phosphonic acids/phosphonates in the synthesis of perovskite NCs and in their structural and optical properties has not been attained so far. This is mostly due to the fact that PAs have been always employed together with additional ligands, such as alkylamines,[14] oleic acid,[14] or trioctylphosphine oxide (TOPO),[20,21,24] therefore generating complex ligand−ligand and ligand−NC interactions.

Received: August 29, 2019
Revised: October 12, 2019
Published: October 14, 2019

DOI: 10.1021/acs.chemmater.9b03529
Chem. Mater. 2019, 31, 9140−9147

In this work, we decided to close this knowledge gap by developing a colloidal approach for the synthesis of $CsPbBr_3$ NCs that employs PAs as the only ligand (see Scheme 1). The

Scheme 1. Colloidal Synthesis of $CsPbBr_3$ NCs Employing Alkylphosphonic Acids

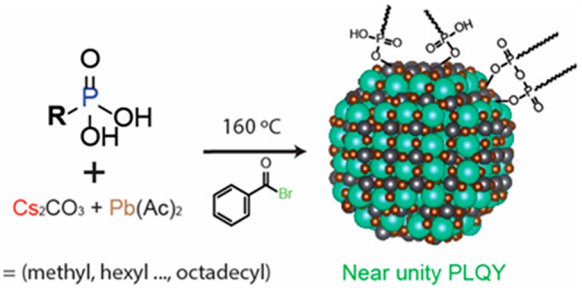

resulting NCs were characterized by a near unity PLQY and almost single exponential PL decay. NMR studies revealed that the surface of the NCs is passivated mainly by phosphonic acid anhydrides and hydrogen phosphonates, where each phosphonate group anchors the NC surface with one oxygen atom, thus bearing a formal −1 charge (see Scheme 1). In addition, the NCs did not exhibit the typical cubic shape of perovskite NCs which are enclosed by (001), ($1\bar{1}0$), and (110) facets of the orthorhombic phase. Note that in the cubic representation, also widely employed as more intuitive, the above facets correspond to (001), (100), and (010), respectively. To avoid confusion, in the following we will always employ the cubic nomenclature for the facets. In the truncated octahedron morphology stabilized with alkylphosphonates new facets are exposed, such as (110) and (111). Density functional theory (DFT) calculations indicate that the phosphonate ligands can efficiently prevent the formation of surface trap states by effectively covering the surface of $CsPbBr_3$ NCs (explaining the high PLQY) and are equally stabilizing the (001) and (110) facets, thus rationalizing the truncated octahedron shape.

EXPERIMENTAL SECTION

Chemicals. Cesium carbonate (Cs_2CO_3, reagent Plus, 99%), lead acetate trihydrate ($Pb(CH_3COO)_2{\cdot}3H_2O$, 99.99%), benzoyl bromide (C_6H_5COBr, 97%), toluene (anhydrous, 99.5%), and octadecene (ODE, technical grade, 90%) were purchased from Sigma-Aldrich. Methylphosphonic acid (MPA), hexylphosphonic acid (HPA), octylphosphonic acid (OPA), tetradecylphosphonic acid (TDPA), and octyldecylphosphonic acid (ODPA) were purchased from PCI synthesis. All chemicals were used without further purification.

Synthesis of $CsPbBr_3$ NCs. A total of 76 mg (0.2 mmol) of lead(II) acetate trihydrate, 16 mg (0.1 mmol) of cesium carbonate, 0.6 mmol of phosphonic acid, and 10 mL of 1-octadecene were mixed in a 25 mL 3-neck flask. The reaction mixture was degassed for 1 h at 110 °C, and then the temperature was raised to 220 °C under a N_2 flux to achieve a full dissolution of the precursors. Subsequently, this (precursor) solution was cooled down to 105 °C and degassed at that temperature for one additional hour. A total of 50 μL of benzoyl bromide diluted in 500 μL of degassed ODE was then injected into the mixture at 160 °C. Immediately after the injection, the reaction was quenched by immersing the flask in an ice−water bath. It is important to specify that if the reaction was allowed to proceed for longer times, partial precipitation of the product occurred already after 30 s. Ethyl acetate, at a volume ratio of 3.5:1 with crude NCs solution, was used to wash the samples. After centrifuging at 6000 rpm for 10 min, the supernatant was discarded, and the NCs were dispersed in toluene (1 mL). The NCs were washed a second time by adding 3.5 mL of ethyl acetate followed by centrifugation at 6000 rpm for 10 min. Eventually, the precipitated NCs were redispersed in toluene and kept in a N_2 filled glovebox for further characterizations.

Optical Characterizations. The UV−visible absorption spectra were recorded using a Varian Cary 300 UV−vis absorption spectrophotometer. The PL spectra were measured on a Varian Cary Eclipse spectrophotometer using an excitation wavelength (λ_{ex}) of 350 nm. Samples were prepared by diluting NC solutions in toluene, in quartz cuvettes with a path length of 1 cm. Photoluminescence decays of dilute NC solutions ($OD_{400\ nm}$ = 0.15) were measured by time-correlated single-photon counting on a Edinburgh Instruments FLS920 spectrofluorometer equipped with a 405 nm laser diode (50 ps pulses) used to excite the NCs. The photoluminescence quantum yields of dilute NC solutions ($OD_{400\ nm}$ = 0.3 ± 0.1) were measured using an integrating sphere, exciting the samples with a 400 nm continuous wave laser diode, and the emitted light was collected with a TM-C10083CA Hamamatsu Mini-Spectrometer.

Transmission Electron Microscopy (TEM). A JEOL JEM-1011 microscope at an accelerating voltage of 100 kV was used to acquire bright field TEM images. The samples were prepared by dropping diluted nanocrystal solution on carbon-coated 200 mesh copper grids. High-resolution TEM (HRTEM) imaging, high-angle annular dark field (HAADF) scanning TEM (STEM) imaging, and energy-dispersive X-ray spectroscopy (EDS) analyses were carried out on a JEOL JEM-2200FS microscope equipped with a Schottky emitter working at an accelerating voltage of 200 kV, a CEOS spherical aberration corrector for the objective lens, and a Bruker Quantax 400 system with a 60 mm^2 XFlash 5060 silicon drift detector (SDD). For HRTEM analyses, the same diluted NCs were drop-cast onto ultrathin carbon/holey carbon-coated 400 mesh copper grids. The EDS spectra were quantified using the Cliff-Lorimer method for Cs Lα, Pb Lα, Br Kα, and P peaks, and the reported STEM-EDS maps were obtained by integrating the intensities over the same peaks.

Dynamic Light Scattering (DLS) Measurements. The solvodynamic diameter of the NCs was determined by a Malvern Zetasizer (Nano Series, Nano ZS) instrument. For each sample, three measurements were taken with 10−20 acquisitions.

X-ray Diffraction (XRD). XRD measurements were performed on a PANalytical Empyrean X-ray diffractometer, with a 1.8 kW Cu Kα ceramic X-ray tube and PIXcel3D 2 × 2 area detector, operating at 45 kV and 40 mA. The samples were prepared by drop-casting onto a zero diffraction silicon substrate.

X-ray Photoelectron Spectroscopy (XPS). This was performed on a Kratos Axis UltraDLD spectrometer, equipped with a monochromatic Al Kα source, which was operated at 20 mA and 15 kV. Concentrated solutions of NCs were drop-cast onto freshly cleaved highly oriented pyrolytic graphite substrates. Survey scans were carried out using an analysis area of 300 × 700 μm and a pass energy of 160 eV. High resolution scans were performed on the same analysis area, but with a pass energy of 10 eV. The Kratos charge neutralizer system was used on all specimens. Spectra were charge corrected to the main line of the carbon 1s spectrum (adventitious carbon) set to 284.8 eV. Spectra were analyzed using CasaXPS software (version 2.3.17).

Nuclear Magnetic Resonance (NMR). NMR spectra were acquired on a Bruker Avance III 400 MHz spectrometer, equipped with a Broad Band Inverse probe (BBI). ^{31}P spectra were performed at 300 K, in chloroform-*d*, by using an inverse gated ^{1}H decoupled ^{31}P NMR sequence (Bruker library). The main acquisition parameters employed were: 64−2048 transients (depending on sample concentration), 64K data points, 4 steady scans, and an interpulses delay of 2 s, over a spectral width of 200.45 ppm (offset at 0.00 ppm), at a fixed receiver gain (2050). NMR experiments at different temperatures (from 300 to 323 K) were performed in toluene-d_8. At each desired temperature, the samples were allowed to equilibrate inside the probe for at least 5 min before acquiring the spectra, keeping the acquisition parameters fixed. All the NMR chemical shifts were referenced to a TEP (triethyl phosphate) 10 mM solution in $CDCl_3$, setting at 0.0 ppm its ^{31}P signal.

DOI: 10.1021/acs.chemmater.9b03529
Chem. Mater. 2019, 31, 9140−9147

Table 1. PAs Employed in the Synthesis of $CsPbBr_3$ NCs and the Corresponding Relevant Properties

PAs employed (ratio)	colloidal stability	size (nm)	PL peak (nm)	fwhm (meV)	PLQY (%)	τ_1 (ns)	τ_1 (%)
TDPA	yes	7.1 ± 1.4	498	125	95.3	4.3	99.1
MPA-ODPA (1:3)	yes	16.7 ± 1.6	518	83	72.4	24.4	57.1
HPA-ODPA (1:3)	yes	9.4 ± 1.1	508	116	92.9	4.1	99.7
TDPA-ODPA (3:1)	yes	7.4 ± 1.0	499	123	96.8	4.4	98.1
OPA	no	>200	522	87	-	-	-
ODPA	no	8.5 ± 1.0	511	94	-	-	-

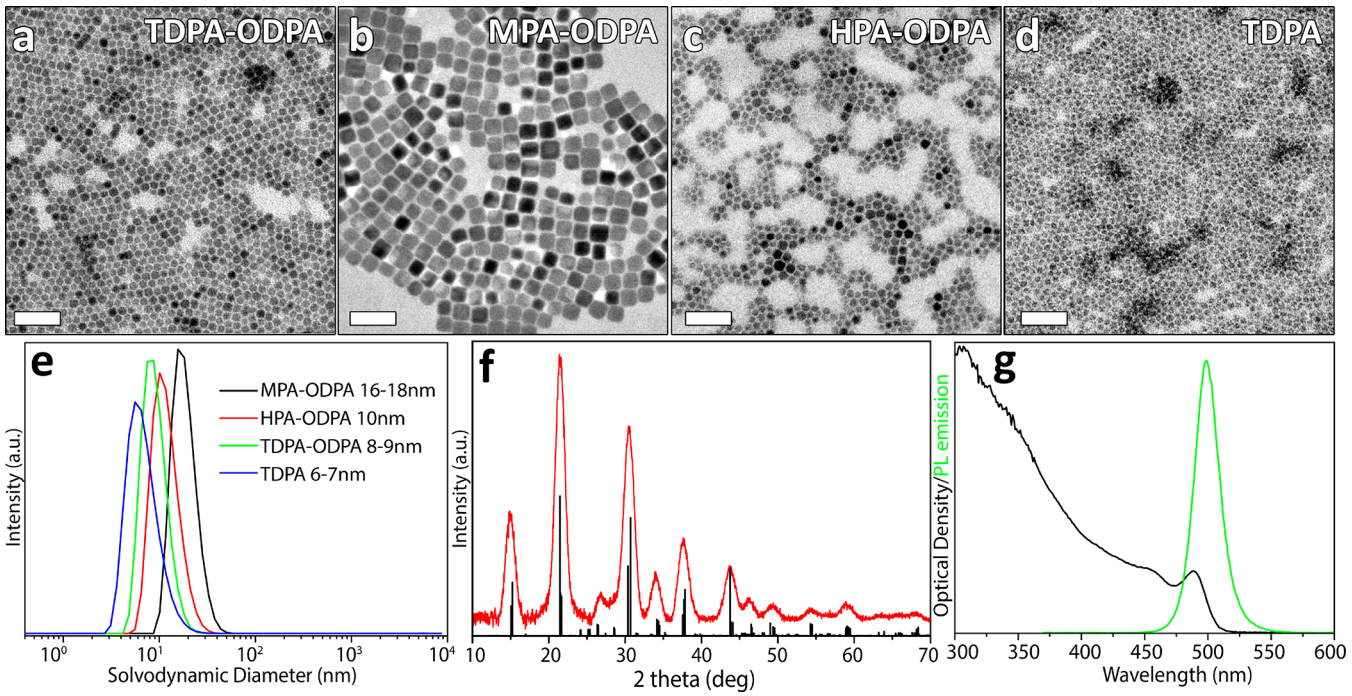

Figure 1. TEM images of $CsPbBr_3$ NCs prepared by using different combinations of PAs: (a) TDPA-ODPA (ratio 3:1), (b) MPA-ODPA (ratio 1:3), (c) HPA-ODPA (ratio 1:3), and (d) TDPA only. The scale bars are 50 nm. (e) Solvodynamic radius of the PA capped NC measured by DLS. (f) XRD pattern and (g) optical absorbance and PL emission of a representative $CsPbBr_3$ NC sample synthesized using TDPA-ODPA (ratio 3:1). In (f) the bulk reflections of $CsPbBr_3$ (ICSD number 98751) are represented by means of black bars.

DFT Calculations. We have carried out atomistic simulations at the density functional theory level using the PBE exchange–correlation functional[25] and a double-ζ basis set plus polarization functions[26,27] on all atoms as implemented in the CP2K 5.1. All structures have been optimized in vacuum. Scalar relativistic effects were incorporated as effective core potential functions in the basis set. Spin–orbit coupling effects were not included, but their impact on the relaxed structural properties was demonstrated to be negligible for similar systems. More details on how the models were built can be found in the main text and in refs 16 and 28.

RESULTS AND DISCUSSION

Synthesis and Structural Characterization. The synthesis of phosphonate capped $CsPbBr_3$ NCs was carried out by modifying the colloidal approach recently reported by our group,[9] in which benzoyl halides are employed as halide precursors. In detail, metal cation precursors (Cs_2CO_3 and $Pb(ac)_2$) were dissolved in 1-octadecene together with the desired alkyl phosphonic acids at 220 °C, and subsequently, the nucleation and growth of the NCs was triggered by the swift injection of benzoyl bromide at 160 °C (see the Experiment Section for details). It is important to highlight that the "pre-heating step" at 220 °C was necessary to obtain a complete solubilization of the precursors, which resulted in fully transparent solutions. Various samples were prepared by employing either PAs having different alkyl chain lengths or combinations of PAs (see Table 1). Our results indicated that the use of either a short-chain PA, such as octylphosphonic acid (OPA, C8), or a long-chain PA, such as octadecyl phosphonic acid (ODPA, C18), did not yield colloidally stable $CsPbBr_3$ NCs (see Figure S1 of the Supporting Information (SI) and Table 1). These findings are different from those that have been recently reported by Tan et al., who could prepare stable LHP NCs in the presence of OPA, Cs–oleate, and trioctylphosphine oxide (TOPO).[20] The comparison suggests that the NCs prepared by Tan et al., unlike ours, were not capped exclusively by OPA. On the other hand, we could prepare colloidally stable NC dispersions either by using PAs with intermediate alkyl chain lengths, such as tetradecyl phosphonic acid (TDPA, C14), or a combination of two PAs (see Table 1 and Figure 1), in which one of the two components is ODPA. TEM and DLS analyses revealed that by changing the chain length of the PAs it was possible to tune the size of $CsPbBr_3$ NCs from ~7 to ~17 nm (Figure 1a–e) with no presence of aggregates. All the NC samples had an orthorhombic $CsPbBr_3$ perovskite structure (ICSD: 98751) and did not contain any secondary phases as evinced by our XRD analysis (Figure 1f and Figure S2).

DOI: 10.1021/acs.chemmater.9b03529
Chem. Mater. 2019, 31, 9140–9147

The PL of PA-capped NCs was found at 498−518 nm with full widths at half-maximum (fwhm) in the range of 83−125 meV (Figure 1g, Figure S2, and Table 1). Interestingly, most of the NC products were characterized by high PLQYs, with values approaching unity for TDPA and TDPA-ODPA capped samples. The samples with PLQYs > 90% exhibited nearly monoexponential PL decays (>98% amplitude weight) with lifetimes of ∼4 ns (Table 1, Table S1 and Figure S3), indicating that phosphonate ligands can effectively suppress nonradiative recombination pathways at the surface of $CsPbBr_3$ NCs.

The TEM images of our samples showed that PA capped NCs had an uncommon truncated octahedron shape (Figures 1 and 2), which has never been previously observed when

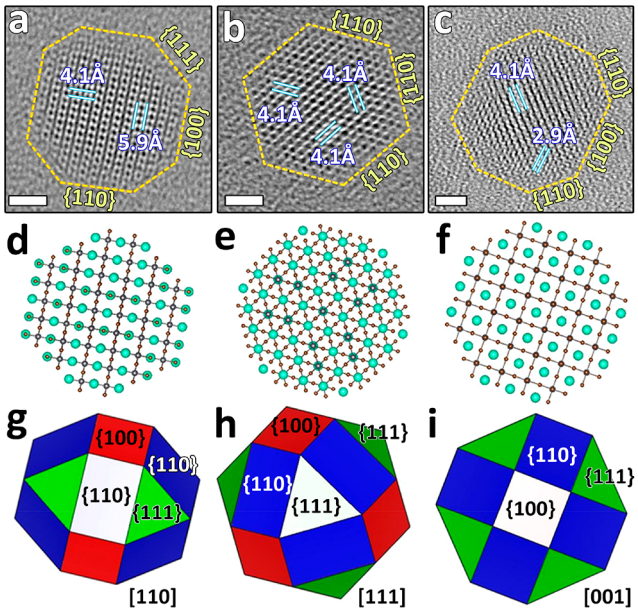

Figure 2. HRTEM images of $CsPbBr_3$ NCs oriented in different zone axes: (a) [110], (b) [111], and (c) [001]. The scale bars are 2 nm. The corresponding (d−f) atomic models built using VESTA[32] (containing Cs (cyan) and Pb (gray) and Br (brown) atoms) and (g−i) polyhedron models with colored facets.

employing alkyl amines or carboxylic acids in "traditional" colloidal synthesis methods (i.e., ligand assisted reprecipitation and hot-injection routes).[3,8−10,14,17,21,29,30] In some cases, our NCs tended to form hexagonal self-assembly patterns on the TEM grids (Figure 1a,d and Figure S4). To further investigate the NCs' morphology and faceting we employed a high-resolution (HR) TEM analysis. Here the analysis corresponds to large NCs, i.e., those prepared using a combination of HPA and ODPA (Figure 1c), whereas smaller NCs tended to degrade quickly under the electron beam during image acquisition (Figure S5). Figure 2a−c reports representative HRTEM images of NCs under commonly observed orientations, with [110], [111], and [001] zone axes, respectively (see also Figure S6 of the Supporting Information). The corresponding atomic models are shown in Figure 2d−f. In addition to the three equivalent (010), (100), and (001) facets, the NCs also exposed several new types of facets, namely, (110) and (111) ones (Figure 2g−i and Figure S7). As mentioned earlier, the faceting of our NC samples is different from that of NCs synthesized by conventional routes, which are known to be enclosed by the equivalent (100), (010), and (001) facets of the cubic phase (ICSD: 98751).[31] We ascribe this unusual faceting to the role that PAs played in passivating the surface of NCs during their growth, as discussed in the DFT section below.

Surface Characterization. To investigate the surface of our NCs, we decided to work on the simplest colloidally stable system we produced, that is, TDPA-capped $CsPbBr_3$ NCs. We initially performed XPS, FTIR, and STEM-EDS analyses which indicated the presence of TDPA at the surface of our perovskite NCs: according to STEM-EDS elemental maps, phosphorus was homogeneously distributed over the whole NCs (Figure S8); FTIR spectra suggested the presence of bound TDPA molecules chelating the surface metal cations (Figure S9);[33,34] and the XPS analysis revealed a Cs/Pb/Br/P molar ratio of 1/1.06/2.19/0.77, which suggested, following the requirements of charge balance, that alkylphosphonates replaced most of Br^- anions on the surface of the NCs, bearing the same formal charge of −1.

To better elucidate the surface chemistry of our NC products and, in particular, the binding motifs of PAs, we also performed an in depth ^{31}P NMR analysis.[35,36] The NMR spectrum of TDPA-capped $CsPbBr_3$ NCs evidenced multiple broad ^{31}P peaks in the range of 15−30 ppm (Figure 3a). If

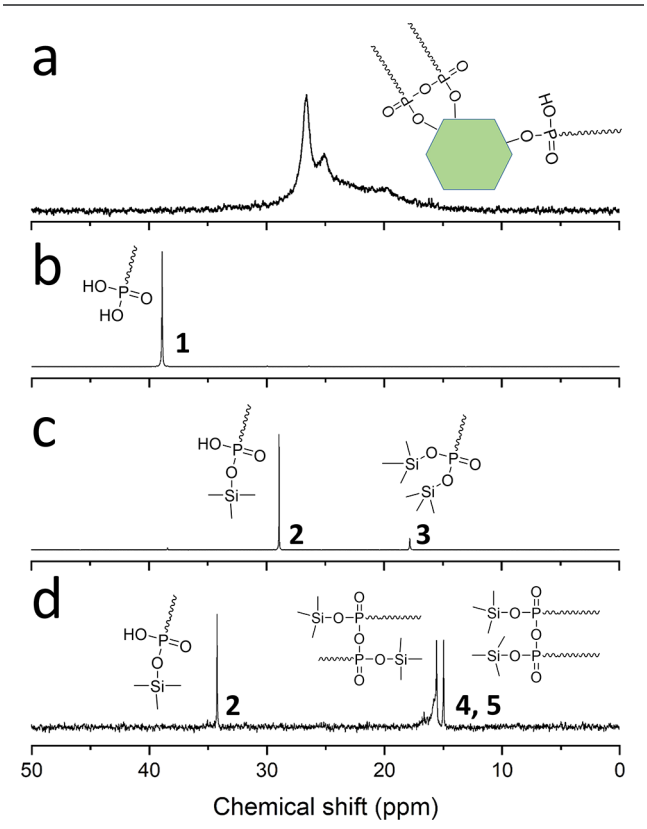

Figure 3. $^{31}P\{^1H$ decoupled$\}$ NMR spectra in $CDCl_3$ of (a) TDPA capped $CsPbBr_3$ NCs, (b) reference "free" TDPA, (c) TDPA after the reaction with chlorotrimethylsilane (TMS-Cl), and (d) TDPA capped $CsPbBr_3$ NCs after the reaction with TMS-Cl.

compared to the sharp ^{31}P singlet of the "free" TDPA (1) NMR spectrum (Figure 3b), the broad peaks characterizing the PA capped LHP NCs indicated a reduced diffusion in solution and a longer correlation time (τ_c), characteristic of TDPA species bound to the surface of the NCs. Also, the

DOI: 10.1021/acs.chemmater.9b03529
Chem. Mater. 2019, 31, 9140−9147

presence of multiple signals suggested that TDPA adopted different surface-binding motifs.[23]

To better elucidate the way TDPA molecules were anchored on the surface of perovskite NCs, we performed control reactions in which chlorotrimethylsilane (TMS-Cl) was reacted with TDPA molecules (Figure 3c) and with the NCs themselves (Figure 3d). This reaction has been previously employed to reveal the binding motifs of alkylphosphonate species on the surface of classical colloidal quantum dots, such as CdSe and PbSe NCs.[19,35,36] That is because TMS-halides and -chalcogenides (i.e., TMS-Se or -S) are able to react with alkylphosphonate species, which are passivating the surface of NCs, forming the corresponding TMS-substituted counterparts (in which TMS groups replace the acid protons of PAs, see Figure 3d and Scheme 2) and precipitating the NCs. The

Scheme 2. Cleavage of the Alkylphosphonate Ligands Bound to the Surface of $CsPbBr_3$ NCs by TMS-Cl

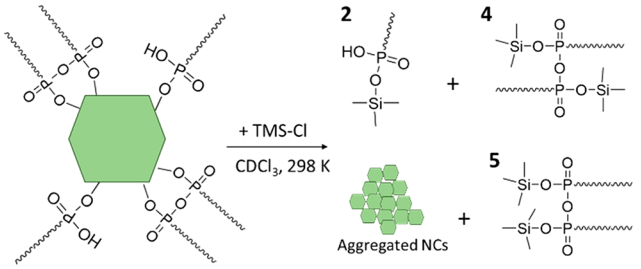

specific species formed upon this reaction, which can be readily detected by ^{31}P NMR analysis, are directly related to the alkyl phosphonate species present on the surface of the NCs (Scheme 2).

Upon reaction of TDPA with TMS-Cl we observed two individual ^{31}P NMR peaks which could be assigned to (**2**) mono- and (**3**) di-TMS substituted TDPA species (see Figure 2c). Namely, these are TMS hydrogen tetradecylphosphonic acid (**2**) and *O*,*O*′-bis(TMS)tetradecylphosphonic acid (**3**), which are the only expected products of this reaction, as also pointed out by Owen et al.[35] On the other hand, after the reaction of TMS-Cl with our perovskite NCs, we observed the formation of three ^{31}P NMR sharp peaks (Figure 3d). In analogy to what was reported by Owen et al., one pair of sharp peaks (13.83 and 14.43 ppm) with similar intensities could be assigned to one pair of isomers of *O*,*O*′-bis(trimethylsilyl)-tetradecylphosphonic acid anhydride (**4**, **5**, see Scheme 2 and Figure 3d).[35] The third peak, at 33.10 ppm, was assigned to (**2**) despite being downfield shifted with respect to what was measured when reacting TMS-Cl with TDPA only (Figure 3c,d). We attributed this shift to a matrix effect, due to the presence of a large excess of TMS-Cl, which acts as a Lewis acid, employed in the reaction with NCs (Figure S10). A similar shift has been also observed in our recent work, where the ^{31}P NMR signal of trioctylphosphine oxide (TOPO) was observed to shift toward higher ppm when exposed to an excess of a Lewis acid (namely, $PbBr_2$ or oleic acid).[21] The broad shoulder signal around 15 ppm (Figure 3d) was tentatively assigned to polyphosphonic anhydrides that may have formed by condensation of phosphonic acids during the synthesis (macromolecules return broad NMR peaks).

Overall, the ^{31}P NMR experiments indicated that TDPA-capped $CsPbB_3$ NCs were passivated mainly by phosphonic acid anhydride and hydrogen phosphonate, in which each alkylphosphonate anchoring group carries a formal −1 charge, in agreement with what emerged from the XPS characterization. We thus attributed the two main broad peaks at 24.84 and 26.12 ppm, that characterize the ^{31}P NMR spectrum of NCs, to these two species, while the weak signal at 19.69 ppm was tentatively assigned to a small amount of polymerized TDPA, bound to the surface of the NCs (Figure 3a).

DFT Results. To reveal how the PA ligands are able to provide an efficient passivation of $CsPbBr_3$ NCs and, at the same time, to induce a truncated octahedron shape, we performed DFT calculations. The $CsPbBr_3$ NCs were modeled as having a 2.5 nm-sided cubic shape presenting two equivalent (001) and four equivalent (110) facets in the cubic representation (Figure S11). This model is slightly different from the observed truncated octahedron shape, but it is computationally more affordable and includes the same facets relevant for our analysis. The (110) facet is terminated by both Cs and Pb ions lying on the same plane, while the (001) type can be either Cs- or Pb-rich terminated. In our calculations we employed a simplified version of the PA ligands by replacing TDPA with shorter alkylic chain ligands, like butyl phosphonate. In these simulations we considered the presence of both hydrogen phosphonate $(HPA)^-$ and phosphonic acid anhydride $(anhy)^{2-}$, which carries two anchoring groups, as emerged from the NMR analysis, and, although not experimentally detected, also phosphonate $(PA)^{2-}$ ligands. The binding affinity (BDE) of the ligands to the NC surface was computed as

$$\mathrm{BDE} = E[\mathrm{NC}] - (E[\mathrm{NC(o)}] + E[\mathrm{BX}_n]) \quad (1)$$

where NC is the core with one facet capped with ligands, NC(o) is the NC with a BX_n vacancy, and BX_n is the dissociated ligand. Here B can be either Cs^+ or Pb^{2+}, and X is the alkylphosphonate counterion. The calculated values of BDE per ligand are reported in Table 2, while the corresponding binding sites are depicted in Figure S11.

Table 2. Computed Values of BDE between Several Types of Metal (Pb or Cs) Phosphonate Groups and the NC Surface[a]

	Pb-rich (001)	Cs-rich (001)	(110)
$Pb(HPA)_2$ (no H-bonded)	52.2	//	44.4
$Pb(HPA)_2$ (H-bonded)	53.2	//	55.1
Cs(HPA)	//	48.5	54.4
Pb(PA)	47.9	//	47.5
Pb(anhy)	68.5	//	65.4

[a]Energies are in kcal/mol.

What emerged from our calculations is that the passivation of a Pb-rich (001) surface with either $Pb(HPA)_2$ or Pb(anhy) moieties is energetically more favorable than passivating a Cs-rich (001) surface with Cs(HPA). This indicates that Pb-rich surfaces are more likely to be stabilized. In addition, both $Pb(HPA)_2$ and Pb(anhy) have similar binding affinities for the (001) and (110) facets, suggesting that the growth rate along these two axes should be equal, explaining the experimental observation of the formation of truncated octahedra. It is interesting to note that the two phosphonate anchoring groups of a single anhydride molecule are expected to occupy two adjacent anion sites at the NC surface. It is apparent from our calculations that this configuration is allowed on both Pb-terminated (001) facets and (110) facets, but less on the Cs-

DOI: 10.1021/acs.chemmater.9b03529
Chem. Mater. 2019, 31, 9140−9147

terminated (001) facets, since on the latter facets the anion sites are too far apart. The formation of truncated octahedra NCs could then be explained considering the presence of Pb(anhy) species which form during the preparation of the precursors and before the hot injection.

The binding of the $Pb(HPA)_2$ on both the (001) and the (110) facets should be further stabilized by the presence of hydrogen bonds between the phosphonate units (see Table 2, first two rows, and Figure S12). The presence of a network of hydrogen bonds, which does not form at the high temperatures used during the synthesis, but most likely after the growth of the NCs, may increase the ligand binding affinity and can explain the evidence (see below and also Table 2) that the ligands are not detached from the surface of our NC even when the NCs are suspended in solvents at high dilutions.

To demonstrate the tolerance of our NCs to the formation of defect states, we have computed the electronic structure of a fully passivated NC with a truncated octahedron shape, exposing all facets as in the experiments (Figure 4a). To

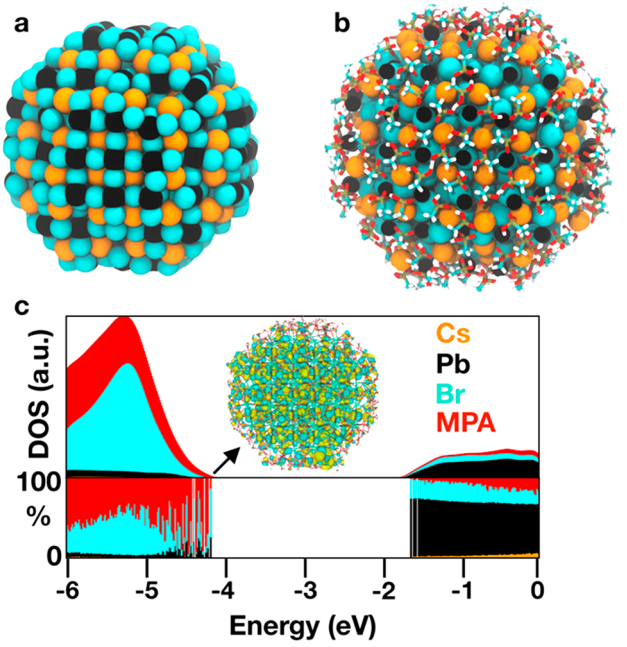

Figure 4. (a) Relaxed $CsPbBr_3$ NC model of the 3.0 nm diameter computed at the DFT/PBE level of theory. Here the phosphonate ligands have been excluded only for pictorial reasons. (b) Same NC model as (a) where also the methylphosphonate (MPA) ligands have been visually included. (c) (top) Projected density of states (PDOS) on each atom and ligand type of the NC model: Cs, orange; Pb, black; Br, turquoise; methylphosphonate, red. A delocalized and free of traps molecular orbital plot of the HOMO state is also shown: (bottom) percentage contribution of each atom or ligand type to each computed molecular orbital.

simplify the model, we have employed only hydrogen phosphonates (i.e., HPA species). Here, we chose the number of phosphonates based on the Cs/Pb/Br/P atomic proportions of 1/1.06/2.19/0.77 found in the XPS elemental analysis. In our model we have the ratio 1/1.12/2.14/1.09. In Figure 4a we show the NC core after relaxing the full structure, whereas in Figure 4b we present the full structure including the phosphonate ligands. In this case, for computational efficiency, we use methylphosphonate (MPA) ligands. What we can observe is that the electronic structure and the geometry of the NC remains substantially intact, even after reconstructing the surface. In Figure 4c we show the electronic structure of this system. Here the VB edge, which is more sensitive to the formation of localized trap states, is fully delocalized (see also Figure S13). Unlike the Cs−oleate case,[21] we observed that an excess of phosphonate ligands introduced subvalence and, thus, shallow, localized states, which do not affect the emission efficiency of these NCs.

Stability Test. In order to assess the colloidal stability of our NC systems we first investigated the PL emission of both "standard" oleylammonium-Br passivated NCs, prepared following the synthesis procedure reported by Protesescu et al.,[8] and TDPA-ODPA capped $CsPbBr_3$ NCs as a function of their concentration in toluene (Figure 5a,b). This test, as

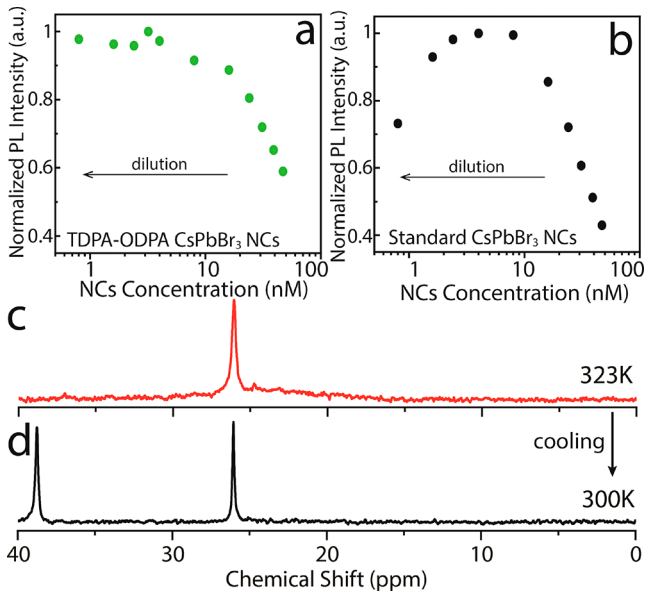

Figure 5. Normalized PL emission intensity as a function of the NC concentration in toluene for (a) TDPA-ODPA and (b) "standard" oleylammonium−Br capped NC samples. ^{31}P NMR spectra in toluene-d_8 of TDPA capped $CsPbBr_3$ NCs (c) heated up to 323 K and subsequently (d) cooled down to 300 K (room temperature).

already reported in detail by Nenon et al., can be used to assess if surface ligands are either strongly or weakly bound to the surface $CsPbBr_3$ NCs.[14] Weakly bound ligands, such as oleylammonium−halide ligand pairs, desorb from the surface of the NCs upon dilution, leaving behind halide vacancies, and, therefore, lowering the final radiative recombination.[14] Our measurements, reported in Figure 5a−b, indicated that (i) at high NC concentrations (100−10 nM), the PL emission of both samples increased in intensity by dilution, most likely due to self-absorption phenomena; (ii) at low NC concentrations (10−1 nM), the PL intensity of standard NCs was observed to decrease by dilution, while that of TDPA-ODPA capped $CsPbBr_3$ NCs remained constant (with PLQY values being around unity). These results confirmed on the one hand the weak binding of oleylammonium−Br^- ligand pairs[14] and on the other hand that alkyl phosphonates ligands were strongly bound to the surface of $CsPbBr_3$ NCs.[36,37]

In order to assess the thermal stability of our PA capped NCs, we performed a control experiment in which TDPA capped $CsPbBr_3$ NCs, dispersed in toluene-d_8, were heated up to 323 K and then cooled down to 300 K (room temperature)

DOI: 10.1021/acs.chemmater.9b03529
Chem. Mater. 2019, 31, 9140−9147

while measuring the corresponding ^{31}P NMR spectrum.[15] Upon heating, the broad ^{31}P signals characterizing TDPA capped NCs (Figure 3a) evolved into a single sharper peak at about 26 ppm (Figure 5c). Furthermore, when cooling the solution back to 300 K the peak at 26 ppm became sharper and a second sharp peak appeared at 37 ppm, which could be assigned to free TDPA (Figure 5d). These results suggested that the heating step led to the irreversible detachment of metal phosphonate ligands from the surface of NCs. This was also supported by the observation that part of the NCs precipitated at the bottom of the NMR tube at the end of the thermal stability test. The presence of free TDPA was tentatively ascribed to the fact that NMR tubes used for this analysis were not hermetically closed and external moisture might have reacted with metal phosphonates to form the corresponding phosphonic acid. Overall our stability tests evidenced that alkylphosphonates are strongly bound to the surface of $CsPbBr_3$ NCs providing a high colloidal stability, but at the same time they have a low thermal stability. Such a low thermal stability is most likely a consequence of the marked ionic character of the NCs: ligands that are strongly bound to the surface of these ionic NCs (as in the present case) can effectively detach surface atoms upon heating.

CONCLUSIONS

We have developed a colloidal route to produce $CsPbBr_3$ NCs by employing alkyl phosphonic acids as the only surfactants. The resulting NCs exhibited an uncommon truncated octahedron shape with new facets exposed. These NCs were characterized by near unity PLQY with nearly monoexponential PL decays. Our NMR analysis revealed the presence of both phosphonic acid anhydride and hydrogen phosphonate species passivating the NCs surface. These ligands were found to provide a high colloidal stability but a low thermal stability (with metal phosphonate species leaving the NC surface upon heating). DFT calculations corroborated the experimental data by demonstrating the high affinity of phosphonate ligands to the NC surface and by showing a similar stabilization energy of the (001) and (110) facets, explaining the formation of a truncated octahedron shape.

Our results, thus, further enrich the knowledge on this class of materials offering a new tool to tune both the morphology and the surface chemistry of LHP NCs. This, in turn, can be exploited to devise and test new chemistry routes to engineer the NC surface, for example, to attempt the synthesis of core–shell heterostructures (i.e., by employing our Pb surface terminated NCs in cation exchange or colloidal atomic layer deposition routes).[38,39]

ASSOCIATED CONTENT

Supporting Information

The Supporting Information is available free of charge on the ACS Publications website at DOI: 10.1021/acs.chemmater.9b03529.

XRD, TEM, and optical data of samples prepared by OPA and ODPA; XRD and optical data of samples synthesized using MPA-ODPA, HPA-ODPA, and TDPA; time-resolved PL decay traces of PA capped NCs; HRTEM analysis of NCs prepared by TDPA-ODPA; polyhedron model of a truncated octahedron $CsPbBr_3$ NC; HAADF-STEM-EDS elemental maps; FT-IR spectra; NMR analysis of trimethylsilyl hydrogen tetradecylphosphonate; and cubic model of a 2.5 nm $CsPbBr_3$ NC, detailed view of the binding sites, and molecular orbital plots of the HOMO and LUMO states (PDF)

AUTHOR INFORMATION

Corresponding Authors

*(I. Infante) E-mail: ivan.infante@iit.it.
*(L. De Trizio) E-mail: luca.detrizio@iit.it.
*(L. Manna) E-mail: liberato.manna@iit.it.

ORCID

Zhiya Dang: 0000-0003-2238-540X
Guilherme Almeida: 0000-0002-0076-8330
Ivan Infante: 0000-0003-3467-9376
Luca De Trizio: 0000-0002-1514-6358
Liberato Manna: 0000-0003-4386-7985

Notes

The authors declare the following competing financial interest(s): Liberato Manna is member of the Advisory Board of Quantum Advanced Solutions LLC, at King Abdullah University of Science and Technology (KAUST), Saudi Arabia.

ACKNOWLEDGMENTS

We would like to thank M. Prato and G. Pugliese for carrying out the XPS and DLS measurements, respectively. We would like to thank also M. Imran for his help in the TEM analysis. We would like to thank Valerio Pinchetti of the Università degli Studi di Milano-Bicocca for measuring the PLQY of our NC systems. I.I. acknowledges The Netherlands Organization of Scientific Research (NWO) through the Innovational Research Incentive (Vidi) Scheme (Grant No. 723.013.002). The computational work was carried out on the Dutch national e-infrastructure with the support of the SURF Cooperative. We also acknowledge funding from the programme for research and Innovation Horizon 2020 (2014-2020) under the Marie Skłodowska-Curie Grant Agreement COMPASS No. 691185.

REFERENCES

(1) Zhang, H.; Wang, X.; Liao, Q.; Xu, Z.; Li, H.; Zheng, L.; Fu, H. Embedding Perovskite Nanocrystals into a Polymer Matrix for Tunable Luminescence Probes in Cell Imaging. *Adv. Funct. Mater.* **2017**, *27*, 1604382.

(2) Chen, X.; Zhang, F.; Ge, Y.; Shi, L.; Huang, S.; Tang, J.; Lv, Z.; Zhang, L.; Zou, B.; Zhong, H. Centimeter-Sized Cs_4PbBr_6 Crystals with Embedded $CsPbBr_3$ Nanocrystals Showing Superior Photoluminescence: Nonstoichiometry Induced Transformation and Light-Emitting Applications. *Adv. Funct. Mater.* **2018**, *28*, 1706567.

(3) D'Innocenzo, V.; Srimath Kandada, A. R.; De Bastiani, M.; Gandini, M.; Petrozza, A. Tuning the Light Emission Properties by Band Gap Engineering in Hybrid Lead Halide Perovskite. *J. Am. Chem. Soc.* **2014**, *136*, 17730−17733.

(4) Stranks, S. D.; Snaith, H. J. Metal-halide perovskites for photovoltaic and light-emitting devices. *Nat. Nanotechnol.* **2015**, *10*, 391.

(5) Luo, X.; Ding, T.; Liu, X.; Liu, Y.; Wu, K. Quantum-Cutting Luminescent Solar Concentrators Using Ytterbium-Doped Perovskite Nanocrystals. *Nano Lett.* **2019**, *19*, 338−341.

(6) Akkerman, Q. A.; Rainò, G.; Kovalenko, M. V.; Manna, L. Genesis, challenges and opportunities for colloidal lead halide perovskite nanocrystals. *Nat. Mater.* **2018**, *17*, 394−405.

(7) Meinardi, F.; Akkerman, Q. A.; Bruni, F.; Park, S.; Mauri, M.; Dang, Z.; Manna, L.; Brovelli, S. Doped Halide Perovskite

DOI: 10.1021/acs.chemmater.9b03529
Chem. Mater. 2019, 31, 9140−9147

Nanocrystals for Reabsorption-Free Luminescent Solar Concentrators. *ACS Energy Lett.* **2017**, *2*, 2368−2377.
(8) Protesescu, L.; Yakunin, S.; Bodnarchuk, M. I.; Krieg, F.; Caputo, R.; Hendon, C. H.; Yang, R. X.; Walsh, A.; Kovalenko, M. V. Nanocrystals of Cesium Lead Halide Perovskites ($CsPbX_3$, X = Cl, Br, and I): Novel Optoelectronic Materials Showing Bright Emission with Wide Color Gamut. *Nano Lett.* **2015**, *15*, 3692−3696.
(9) Imran, M.; Caligiuri, V.; Wang, M.; Goldoni, L.; Prato, M.; Krahne, R.; De Trizio, L.; Manna, L. Benzoyl Halides as Alternative Precursors for the Colloidal Synthesis of Lead-Based Halide Perovskite Nanocrystals. *J. Am. Chem. Soc.* **2018**, *140*, 2656−2664.
(10) Shamsi, J.; Urban, A. S.; Imran, M.; De Trizio, L.; Manna, L. Metal Halide Perovskite Nanocrystals: Synthesis, Post-Synthesis Modifications, and Their Optical Properties. *Chem. Rev.* **2019**, *119*, 3296−3348.
(11) Quarta, D.; Imran, M.; Capodilupo, A.-L.; Petralanda, U.; van Beek, B.; De Angelis, F.; Manna, L.; Infante, I.; De Trizio, L.; Giansante, C. Stable Ligand Coordination at the Surface of Colloidal $CsPbBr_3$ Nanocrystals. *J. Phys. Chem. Lett.* **2019**, *10*, 3715−3726.
(12) De Roo, J.; Ibáñez, M.; Geiregat, P.; Nedelcu, G.; Walravens, W.; Maes, J.; Martins, J. C.; Van Driessche, I.; Kovalenko, M. V.; Hens, Z. Highly Dynamic Ligand Binding and Light Absorption Coefficient of Cesium Lead Bromide Perovskite Nanocrystals. *ACS Nano* **2016**, *10*, 2071−2081.
(13) Ripka, E. G.; Deschene, C. R.; Franck, J. M.; Bae, I.-T.; Maye, M. M. Understanding the Surface Properties of Halide Exchanged Cesium Lead Halide Nanoparticles. *Langmuir* **2018**, *34*, 11139−11146.
(14) Nenon, D. P.; Pressler, K.; Kang, J.; Koscher, B. A.; Olshansky, J. H.; Osowiecki, W. T.; Koc, M. A.; Wang, L.-W.; Alivisatos, A. P. Design Principles for Trap-Free $CsPbX_3$ Nanocrystals: Enumerating and Eliminating Surface Halide Vacancies with Softer Lewis Bases. *J. Am. Chem. Soc.* **2018**, *140*, 17760−17772.
(15) Imran, M.; Ijaz, P.; Goldoni, L.; Maggioni, D.; Petralanda, U.; Prato, M.; Almeida, G.; Infante, I.; Manna, L. Simultaneous Cationic and Anionic Ligand Exchange For Colloidally Stable $CsPbBr_3$ Nanocrystals. *ACS Energy Lett.* **2019**, *4*, 819−824.
(16) Bodnarchuk, M. I.; Boehme, S. C.; ten Brinck, S.; Bernasconi, C.; Shynkarenko, Y.; Krieg, F.; Widmer, R.; Aeschlimann, B.; Günther, D.; Kovalenko, M. V.; Infante, I. Rationalizing and Controlling the Surface Structure and Electronic Passivation of Cesium Lead Halide Nanocrystals. *ACS Energy Lett.* **2019**, *4*, 63−74.
(17) Krieg, F.; Ochsenbein, S. T.; Yakunin, S.; ten Brinck, S.; Aellen, P.; Süess, A.; Clerc, B.; Guggisberg, D.; Nazarenko, O.; Shynkarenko, Y.; Kumar, S.; Shih, C.-J.; Infante, I.; Kovalenko, M. V. Colloidal $CsPbX_3$ (X = Cl, Br, I) Nanocrystals 2.0: Zwitterionic Capping Ligands for Improved Durability and Stability. *ACS Energy Lett.* **2018**, *3*, 641−646.
(18) Yang, D.; Li, X.; Zhou, W.; Zhang, S.; Meng, C.; Wu, Y.; Wang, Y.; Zeng, H. $CsPbBr_3$ Quantum Dots 2.0: Benzenesulfonic Acid Equivalent Ligand Awakens Complete Purification. *Adv. Mater.* **2019**, *0*, 1900767.
(19) Woo, J. Y.; Lee, S.; Lee, S.; Kim, W. D.; Lee, K.; Kim, K.; An, H. J.; Lee, D. C.; Jeong, S. Air-Stable PbSe Nanocrystals Passivated by Phosphonic Acids. *J. Am. Chem. Soc.* **2016**, *138*, 876−883.
(20) Tan, Y.; Zou, Y.; Wu, L.; Huang, Q.; Yang, D.; Chen, M.; Ban, M.; Wu, C.; Wu, T.; Bai, S.; Song, T.; Zhang, Q.; Sun, B. Highly Luminescent and Stable Perovskite Nanocrystals with Octylphosphonic Acid as a Ligand for Efficient Light-Emitting Diodes. *ACS Appl. Mater. Interfaces* **2018**, *10*, 3784−3792.
(21) Almeida, G.; Ashton, O. J.; Goldoni, L.; Maggioni, D.; Petralanda, U.; Mishra, N.; Akkerman, Q. A.; Infante, I.; Snaith, H. J.; Manna, L. The Phosphine Oxide Route toward Lead Halide Perovskite Nanocrystals. *J. Am. Chem. Soc.* **2018**, *140*, 14878−14886.
(22) Xuan, T.; Yang, X.; Lou, S.; Huang, J.; Liu, Y.; Yu, J.; Li, H.; Wong, K.-L.; Wang, C.; Wang, J. Highly stable $CsPbBr_3$ quantum dots coated with alkyl phosphate for white light-emitting diodes. *Nanoscale* **2017**, *9*, 15286−15290.
(23) Brown, A. A. M.; Hooper, T. J. N.; Veldhuis, S. A.; Chin, X. Y.; Bruno, A.; Vashishtha, P.; Tey, J. N.; Jiang, L.; Damodaran, B.; Pu, S. H.; Mhaisalkar, S. G.; Mathews, N. Self-assembly of a robust hydrogen-bonded octylphosphonate network on cesium lead bromide perovskite nanocrystals for light-emitting diodes. *Nanoscale* **2019**, *11*, 12370−12380.
(24) Yang, X.; Zhang, X.; Deng, J.; Chu, Z.; Jiang, Q.; Meng, J.; Wang, P.; Zhang, L.; Yin, Z.; You, J. Efficient green light-emitting diodes based on quasi-two-dimensional composition and phase engineered perovskite with surface passivation. *Nat. Commun.* **2018**, *9*, 570.
(25) Perdew, J. P.; Burke, K.; Ernzerhof, M. Generalized Gradient Approximation Made Simple. *Phys. Rev. Lett.* **1996**, *77*, 3865−3868.
(26) VandeVondele, J.; Hutter, J. Gaussian basis sets for accurate calculations on molecular systems in gas and condensed phases. *J. Chem. Phys.* **2007**, *127*, 114105.
(27) Hutter, J.; Iannuzzi, M.; Schiffmann, F.; VandeVondele, J. cp2k: atomistic simulations of condensed matter systems. *Wiley Interdiscip. Rev.: Comput. Mol. Sci.* **2014**, *4*, 15−25.
(28) ten Brinck, S.; Infante, I. Surface Termination, Morphology, and Bright Photoluminescence of Cesium Lead Halide Perovskite Nanocrystals. *ACS Energy Lett.* **2016**, *1*, 1266−1272.
(29) Nedelcu, G.; Protesescu, L.; Yakunin, S.; Bodnarchuk, M. I.; Grotevent, M. J.; Kovalenko, M. V. Fast Anion-Exchange in Highly Luminescent Nanocrystals of Cesium Lead Halide Perovskites ($CsPbX_3$, X = Cl, Br, I). *Nano Lett.* **2015**, *15*, 5635−5640.
(30) Imran, M.; Ijaz, P.; Baranov, D.; Goldoni, L.; Petralanda, U.; Akkerman, Q.; Abdelhady, A. L.; Prato, M.; Bianchini, P.; Infante, I.; Manna, L. Shape-Pure, Nearly Monodispersed $CsPbBr_3$ Nanocubes Prepared Using Secondary Aliphatic Amines. *Nano Lett.* **2018**, *18*, 7822−7831.
(31) Cottingham, P.; Brutchey, R. L. On the crystal structure of colloidally prepared $CsPbBr_3$ quantum dots. *Chem. Commun.* **2016**, *52*, 5246−5249.
(32) Momma, K.; Izumi, F. VESTA 3 for three-dimensional visualization of crystal, volumetric and morphology data. *J. Appl. Crystallogr.* **2011**, *44*, 1272−1276.
(33) Luschtinetz, R.; Seifert, G.; Jaehne, E.; Adler, H.-J. P. Infrared Spectra of Alkylphosphonic Acid Bound to Aluminium Surfaces. *Macromol. Symp.* **2007**, *254*, 248−253.
(34) Son, J. G.; Choi, E.; Piao, Y.; Han, S. W.; Lee, T. G. Probing organic ligands and their binding schemes on nanocrystals by mass spectrometric and FT-IR spectroscopic imaging. *Nanoscale* **2016**, *8*, 4573−4578.
(35) Owen, J. S.; Park, J.; Trudeau, P.-E.; Alivisatos, A. P. Reaction Chemistry and Ligand Exchange at Cadmium−Selenide Nanocrystal Surfaces. *J. Am. Chem. Soc.* **2008**, *130*, 12279−12281.
(36) Gomes, R.; Hassinen, A.; Szczygiel, A.; Zhao, Q.; Vantomme, A.; Martins, J. C.; Hens, Z. Binding of Phosphonic Acids to CdSe Quantum Dots: A Solution NMR Study. *J. Phys. Chem. Lett.* **2011**, *2*, 145−152.
(37) Smock, S. R.; Williams, T. J.; Brutchey, R. L. Quantifying the Thermodynamics of Ligand Binding to $CsPbBr_3$ Quantum Dots. *Angew. Chem.* **2018**, *130*, 11885−11889.
(38) Ithurria, S.; Talapin, D. V. Colloidal Atomic Layer Deposition (c-ALD) using Self-Limiting Reactions at Nanocrystal Surface Coupled to Phase Transfer between Polar and Nonpolar Media. *J. Am. Chem. Soc.* **2012**, *134*, 18585−18590.
(39) De Trizio, L.; Manna, L. Forging Colloidal Nanostructures via Cation Exchange Reactions. *Chem. Rev.* **2016**, *116*, 10852−10887.

DOI: 10.1021/acs.chemmater.9b03529
Chem. Mater. 2019, 31, 9140−9147